A NOVEL SYNCHROTRON RADIATION INTERFEROMETER FOR THE AUSTRALIAN SYNCHROTRON*

K.P. Wootton#, School of Physics, Monash University, Clayton 3800, VIC, Australia
M.J. Boland, Australian Synchrotron, Clayton 3168, VIC, Australia

Abstract

A new arrangement for the synchrotron radiation interferometer was proposed. The Young's-type interferometer is composed of two independent and optically identical paths, each with a single slit on a motorised translating stage. This arrangement permits rapid scanning of the profile of fringe visibility as a function of slit separation. The interferometer was used on two beamlines at the Australian Synchrotron, the optical diagnostic and infrared beamlines, to measure the coherence of the photon beam created by the electron beam source, for normal and low emittance couplings. A large change in fringe visibility was observed, proving the experimental arrangement. The interferometer was validated in the measurement of the width of a range of hard-edged single slits, ranging over an order of magnitude in diameter.

INTRODUCTION

The synchrotron radiation interferometer is an established optical diagnostic of many modern electron storage rings [1]. The technique leverages the partial spatial coherence of synchrotron radiation to determine the maximum size of the electron beam. The shape and size of the photon source produce a complementary profile (Fourier transform) of interference fringe visibilities.

The measured quantity of visibility of interference fringes with slit separation is typically determined by interchanging a series of double slits, at various separations. Thereafter, a single slit separation is fixed and the fringe visibility changes over time with electron beam size.

This work introduces an arrangement whereby two independent single slits – mounted on motorised translation stages – can be readily scanned transversely across the synchrotron radiation profile.

THEORY

Theory governing synchrotron radiation interferometers is well-documented, and will be outlined here briefly.

The experimental apparatus is essentially Young's double slit interferometer. Two singles slits are used, each of half-width a. The slits are at a transverse separation d, corresponding to a very large angular separation requiring a lens to form an image of the diffraction pattern at a distance of R_1 beyond the slits. The intensity distribution of the diffracted pattern $I(y)$ is described by the relationship [2]:

$$I(y) = I_0 \mathrm{sinc}^2\left(\frac{2\pi a}{\bar{\lambda}R_1}y\right)\left[1+|\gamma(\nu)|\cos\left(\frac{2\pi d}{\bar{\lambda}R_1}y+\varphi\right)\right], \quad (1)$$

where the photon beam is assumed quasi-monochromatic about some central wavelength $\bar{\lambda}$.

The magnitude of the complex degree of coherence $|\gamma(\nu)|$ is a function of the spatial frequency $\nu(d,\bar{\lambda})$ [2]. The slit separation d alone will be varied. For slits illuminated with light of equal intensity, $|\gamma(d)|$ is equivalent to the measured fringe visibility.

For a thermal Gaussian photon source, $|\gamma(d)|$ is given by [3]:

$$|\gamma(d)| = e^{-\frac{d^2}{2\sigma_d{}^2}}, \quad (2)$$

where σ_d denotes one standard deviation width of the measured profile of $|\gamma(d)|$ with slit separation. The size of the photon source σ_y is then given by [3]:

$$\sigma_y = \frac{\bar{\lambda}R_0}{2\pi\sigma_d}, \quad (3)$$

where R_0 is the propagation distance from the source to the double slit.

A hard-edged pinhole aperture was also imaged. The profile of visibility $|\gamma(d)|$ for such a source imaged by a double slit interferometer is described by [4]:

$$|\gamma(d)| = \frac{|\sin\xi|}{\xi}, \quad \xi = \frac{\pi\rho}{\bar{\lambda}R_0}d, \quad (4)$$

where the pinhole source is of diameter ρ.

INTERFEROMETER CONSTRUCTION

As far as is known, the interferometer as constructed is unique in the world. Theoretically, it measures the coherence of the photon beam in an identical manner to other SR interferometers. The feature of this arrangement is that with mechanisation, each of the single slits can be independently scanned across the photon beam to map the fringe visibility with increasing slit separation. Hence, this interferometer should be sensitive over a much larger range of electron beam size than interferometers with a fixed slit separation. The interferometer is illustrated schematically in Fig. 1 below.

The premise of this layout is to exert independent control over the two independent single slits, converging the two single slit diffraction patterns to form the image of a double slit pattern.

Two configurations for the lenses were explored. Initially, a lens was placed on each path, immediately following the single slit.

*Work supported by Australian Synchrotron studentship.
#kent.wootton@synchrotron.org.au

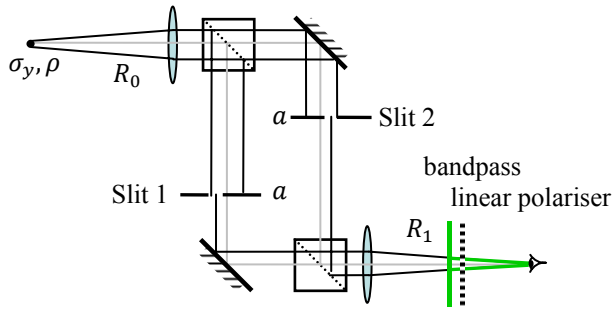

Figure 1: SR interferometer, illustrating two separate single slits, each offset by distance d / 2 from the central axis.

It was found to be more effective, and much simpler to position a lens before and after the beamsplitter arrangement, as illustrated in Fig. 1. The operation of the interferometer was largely insensitive to the centres or tilts of the lenses. The positioning of the two lenses resembles Thompson and Wolf's diffractometer [5].

Components

The beam is split and recombined equally in power using an unpolarised beamsplitter cube. Two planar mirrors of surface roughness λ/10 are used in steering the beam. Planoconvex lenses of diameter 25.4 mm and effective focal length 300 mm were selected. Variable aperture single slits were selected, with a typical aperture used between 200-300 µm.

A laser line bandpass filter of $\bar{\lambda}$ = 532 nm, 10 nm FWHM bandpass is optimised for the broadband visible antireflection coatings. Retrospectively, this is deemed too tight – a filter of up to 60 nm may not appreciably degrade the visibility of the central fringes [6]. A polarised beamsplitter cube was used for rejection of the π-mode polarisation of synchrotron radiation as it has a phase difference of π with the σ-mode, which would diminish the observed fringe visibility [1].

Linear translation stages were matched with actuators of a travel range of 12mm. The APT motor controllers feature USB connections and ActiveX control software, which was incorporated directly into MATLAB scripts.

Image acquisition was accomplished using a greyscale CCD flea camera, interfaced to EPICS.

The most difficult aspect of construction is alignment, especially minimising the path length difference to within the coherence length of the bandpass filter of only 28 µm. A streak camera could be very beneficial.

Beamlines

The optical diagnostic beamline (ODB) at the Australian Synchrotron is designed to cater principally to the longitudinal profile of the photon beam. It serves a suite of instruments, including a streak camera, bunch purity monitor and fill pattern monitor [7]. To deliver light to these instruments, a biconvex lens forms an image of the photon beam source over the optical table [8]. The distance between this virtual source and interferometer, R_0 is limited to at most 2-3 metres. Most SR interferometers have $R_0 \approx 10$ m.

The beamline front end has several apertures, with the crotch absorber the limiting aperture: 5 mm (2.8 mrad) vertical × 10 mm (5.6 mrad) horizontal. This is a standard crotch absorber used for bending magnet x-ray beamlines, but is too narrow to pass the vertical fan of optical synchrotron radiation, even at the VUV limit. Simulations made in Synchrotron Radiation Workshop demonstrate that passing the full vertical fan (3σ, 99.8% power) at 532 nm requires a vertical aperture of 15 mm (8.4 mrad).

The infrared beamline at the Australian Synchrotron has a much larger angular acceptance than the optical beamline. Bending magnet and edge radiation are extracted using a slotted mirror of 17.3 mrad vertical × 60.2 mrad horizontal [9]. A centrally positioned slot of 2.3 mrad (3 mm) passes the hot x-ray fan.

MEASUREMENTS

A goal of this interferometer is to directly confirm the vertical beam size, and hence the emittance coupling ratio of the storage ring beam. Indirect measurements using the Touschek lifetime have been made, giving a minimal emittance coupling of 0.009% [10].

Fringe visibilities were assigned for each slit separation by fitting Equation (1) to the measured visibility distribution, using a Levenberg-Marquhart technique. This is illustrated in Fig. 2 below.

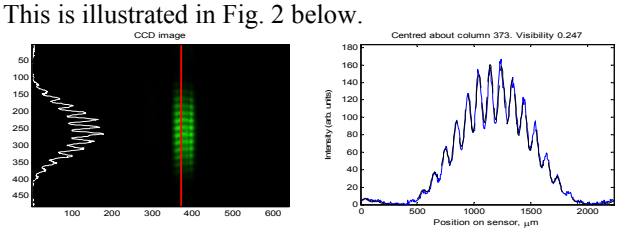

Figure 2: Fitting to determine fringe visibility. Blue: slice of measured interferogram, black: Equation (1), fitted for a visibility of 0.25.

Pinhole verification

The interferometer was arranged to image a selection of circular pinholes, the results of which are presented in Fig. 5. The propagation distance R_0 and separation of camera and objective R_1 were both 300 mm. The source pinhole was illuminated by a 600 µm diameter multimode optical fibre, positioned immediately behind the pinhole. To increase the measured intensity the integration time of the CCD was set as high as 1500 ms for pinhole 1.

Once aligned, each scan of approximately 20 slit separations was taken in less than five minutes.

The diameters of the pinholes were calibrated by single slit diffraction. A summary of the results is shown in Table 1 below.

Table 1: Measurement of Pinhole Diameter ρ

Pinhole -	Single Slit Diffraction [µm]	SR Interferometer [µm]
1	15 ± 2	15 ± 2
2	42 ± 3	38 ± 2
3	174 ± 10	171 ± 5

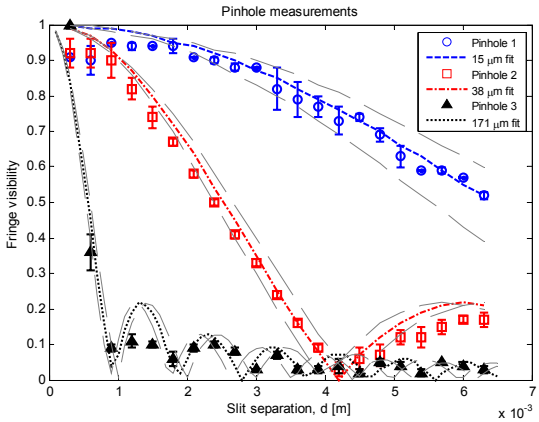

Figure 3: Measured profiles of fringe visibility for three pinhole sources. For uncertainties refer to Table 1.

Infrared Beamline

As the ODB mirror accepts light only above the orbit plane of the ring, measurements of the profile of synchrotron radiation were undertaken on the infrared microspectroscopy beamline. The beam emittance coupling was varied from nominal user coupling of 1% to a minimum coupling. The interferometer was at an effective distance R_0 of 1.00 m. At a single fixed slit separation of 3 mrad, the fringe visibility was seen to increase as the coupling was reduced. This is illustrated in Fig. 4 below.

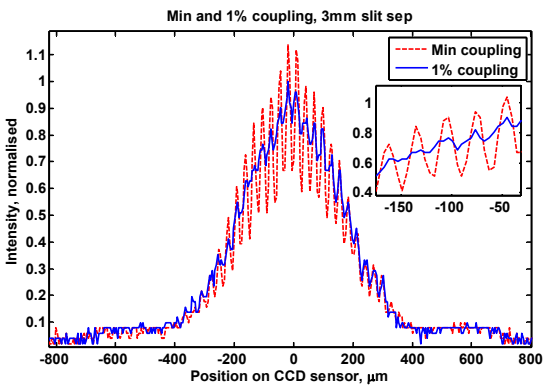

Figure 4: Observed increase in visibility with reduction of coupling. $|\gamma(3)_{1\%}| = 0.05, |\gamma(3)_{min}| = 0.35$.

Figure 5 below shows the profile of visibility with slit separation.

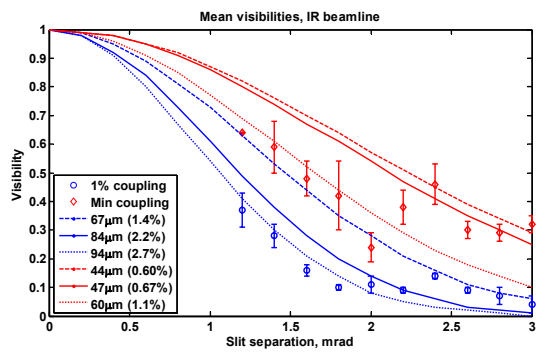

Figure 5: Fringe visibility profiles with variation in emittance coupling. (red: minimal, blue: 1% coupling).

DISCUSSION

The results of the pinhole measurement in Fig. 3 demonstrate the high dynamic range of the setup to measure source size, over at least an order of magnitude. A source size of 15 μm can be determined to ± 2 μm.

The results presented in Figs. 4 and 5 demonstrate qualitatively that the interferometer can image a synchrotron radiation bending magnet source. The couplings quoted in Fig. 5 compare poorly with other measurements. It is believed that the fringe visibility is degraded by the three infrared-transparent windows in the optical path, that are not optically flat at visible wavelengths.

The interferometer installed on the optical table is compact, with a footprint of approximately 0.2 m × 0.7 m. The dimensions would be scalable to suit larger transverse size, or greater propagation distance. Once aligned, scans require no user intervention to change slit separation. As such, a permanent diagnostic could be mounted near the photon source, within the accelerator tunnels.

CONCLUSION

The new arrangement for the synchrotron radiation interferometer has been demonstrated to give accurate measurements of three pinholes ranging in size over an order of magnitude. We have demonstrated a measurement of a pinhole source 15 ± 2 μm.

A measurement of the vertical size of the storage ring electron beam was made on the infrared beamline. The observed fringe visibility defined a source much larger than determined by other direct measurements.

We aim to implement the interferometer as a diagnostic in the future, on an accommodating beamline.

ACKNOWLEDGEMENT

This work was undertaken on the optical diagnostic, and infrared microspectroscopy beamlines at the Australian Synchrotron, Victoria, Australia.

REFERENCES

[1] T. Mitsuhashi, PAC'97, Vancouver, May 1997, 3V016, p. 766-68 (1997).
[2] M. Katoh and T. Mitsuhashi, PAC'99, New York, March 1999, WEP22, p. 2307-09 (1999).
[3] J. Corbett et al., PAC'09, Vancouver, May 2009, TH6REP033. (2009).
[4] D.M. Paganin, Coherent X-Ray Optics, Clarendon Press, Oxford, p. 34 (2006).
[5] M. Born and E. Wolf, Principles of Optics, 7th Ed., p. 578, (1999).
[6] L. Basano, et al., Applied Optics, (2003) 42 (31) 6239.
[7] D.J. Peake, et al., Nucl. Inst. and Methods A, 589 (2008) 143.
[8] M.J. Boland et al., EPAC'06, Edinburgh, June 2006, THPLS002, p. 3263 (2006).
[9] D. Creagh, J. McKinlay, and P. Dumas, Vibrational Spectroscopy, (2006) 41, 213.
[10] R. Dowd, et al., PAC'09, Vancouver, TH6PFP008 (2009).